Eur. Phys. J. A **26**, 33–40 (2005)
DOI 10.1140/epja/i2005-10118-y

THE EUROPEAN PHYSICAL JOURNAL A

Electromagnetic response and breakup of light weakly bound nuclei in a dicluster model

L. Fortunato[a] and A. Vitturi

Dipartimento di Fisica "G. Galilei", Università di Padova and INFN, via Marzolo 8, I-35131 Padova, Italy

Received: 13 June 2005 / Revised version: 8 July 2005 /
Published online: 11 October 2005 –
Communicated by C. Signorini

Abstract. The light weakly bound nucleus ^{7}Li is studied within a dicluster $\alpha + t$ picture. Different observables obtained within our simple model are compared with previous calculations and experiments showing good agreement. In particular, we calculate dipole and quadrupole electromagnetic response to the continuum. The energy distribution of $B(E\lambda)$ values are consistent with the energy-weighted molecular sum rule and display a sizable contribution of non-resonant character arising from the weak binding property. The corresponding form factors for excitations to the continuum are used in a semiclassical coupled-channel scheme to get estimates for the breakup cross-section in a heavy-ion reaction. The nuclear contribution is found to play an important role in the process for bombarding energies around the Coulomb barrier. The masses and charges ratios of the two clusters are shown to lead to features of the cluster halo that may significantly differ from the one usually associated with one-nucleon haloes.

PACS. 21.60.Gx Cluster models – 24.10.Eq Coupled-channel and distorted-wave models – 25.60.Gc Breakup and momentum distributions

1 Introduction

A distinctive feature of nuclear systems along the neutron drip line is the concentration of multipole strength at excitation energies just above the continuum threshold. This concentration of strength (mainly of dipole or quadrupole nature) is directly measured in breakup reactions, but it has strong dynamical effects also on other processes, such as elastic scattering or sub-barrier fusion reactions. It has been proved that this peculiar feature is associated with the weakly bound nature of most nuclei at the drip line ([1–5]). Within a dicluster description of a weakly bound nucleus (where in the simplest case one of the clusters may be a single nucleon) the quantum state that describes the system lies very close to the threshold for separation into the two subsystems. The wave function for the relative motion associated with such a state (and hence its distribution of matter) extends to large radii, spreading far outside the walls of the intercluster potential well (this is valid already at the level of a square well potential, and it is even more evident for a realistic potential with a diffused surface). This establishes the opportunity to set a matching between the bound wave function and some scattering state in the (low-lying) continuum whose typical wavelength roughly corresponds to the spatial extension of the bound state wave function. As a consequence, the resulting electromagnetic response shows a marked concentration of strength in the threshold region at an excitation energy directly correlated to the binding energy. With the specific scaling that depends on the angular momentum of the initial state, as well as on the neutron or proton character of the halo state, the energy corresponding to the maximum of the strength distribution follows approximately a linear behaviour on the binding energy [6], while the total dipole strength at the threshold depends approximatively on the inverse of the binding energy and tends therefore to magnify its effects as one approaches the drip lines.

The picture outlined above finds its simplest application in the case of single particle haloes [7,1], where, in a mean-field approach, it is the last unpaired nucleon that is responsible for the halo distribution, but it can be extended to the case of light weakly bound dicluster nuclei to describe excitations to continuum states that lead to cluster breakup. A number of experiments have been pursued in recent years, for instance, on the study of breakup of Li isotopes [8–11]. We will take as a paradigmatic example the case of the nucleus ^{7}Li, whose ground state is well described in terms of interacting α and triton clusters, which characterize the lowest continuum threshold (at 2.467 MeV). The basic necessary assumption is that the excited states, both bound and unbound, are also described within the same dicluster picture, assuming the

[a] e-mail: fortunat@pd.infn.it

two clusters to be frozen. The excitation process is therefore reduced to a transition in the wave function describing the cluster-cluster relative motion.

This simple model for the threshold strength is modified when the system displays, in the low-energy continuum, true resonant states in addition to the non-resonant part. This is, for example, precisely the case of ^{7}Li which has the $7/2^-$ and $5/2^-$ states at 4.652 MeV and 6.604 MeV, respectively. Within the cluster picture these states correspond to narrow resonances in the relative motion with angular momentum $\ell = 3$. *Ad hoc* formalisms, which only include either the resonances or the non-resonant continuum, may therefore be inadequate to describe the full process. In a proper treatment of the response to the continuum both resonant and non-resonant contributions arise in a natural way and may have comparable strengths. As an example of such an approach we recall the recent work of Kelly and collaborators [8], who analyzed experimental data within a CDCC approach [12], in which the continuum is discretized. The binning of the continuum is however not optimal due to computational limitations, a problem that as we will see, is not present in our model. CDCC calculations usually consider only a few energy bins in the relevant low-energy region, while our approach can easily accommodate for thousands of bins in the same energy range. Other CDCC calculations for ^{7}Li breakup are found in ref. [13].

In our calculation, the form factors for excitations to the continuum have been used in a semiclassical coupled-channel scheme to get estimates for the breakup cross-section. As an example, we have chosen the specific reaction $^7\mathrm{Li} + {}^{165}\mathrm{Ho}$ for which subbarrier fusion data are available and for which estimates of breakup probabilities are important for the interpretation of the data [14]. Since there are indications that the nuclear field plays a non-negligible role [15], both Coulomb and nuclear contributions are included and their relative importance is analyzed. The non-resonant contribution to the cross-section is found to provide a sizable fraction of the total cross-section. Due to the strong nuclear component, the quadrupole breakup process is predicted to dominate over the dipole. Since optical parameters for holmium are not available, we have also tested our model against other calculations [8] for the reaction $^7\mathrm{Li} + {}^{208}\mathrm{Pb}$, finding good agreement.

2 Dicluster description of ^{7}Li

Walliser and Fliessbach [16] discuss a cluster picture for ^{7}Li, in which the constituents of the nucleus (the α and t particles) are treated as elementary, that is without internal structure, but not necessarily point-like. They obtain considerable agreement with experimental data and we conform, in principle, to their model. The main difference is the choice of the potential to be used to determine the relative motion of the cluster. In similarity with the usual single-particle case, our effective α-t potential

$$V_{\alpha\text{-}t}(r) \;=\; V_{coul}(r) + V_{WS}(r) + V_{\mathbf{l}\cdot\mathbf{s}}(r) \qquad (2.1)$$

Table 1. Comparison of calculated and experimental quantities. The second column shows our results, while the third are various experimental data. The last contains calculations performed by other authors. The apices in square brackets indicate the references.

Quantity	This work	Experiments	Other works
$\langle r^2\rangle_{ch}^{1/2}$ (fm)	2.44	$2.55(0.07)^{[16]}$ $2.39(0.03)^{[16]}$	$2.43^{[16,21]}$ $2.55^{[22]}$
Q_{el} (fm^2)	-3.77	$-3.8(1.1)^{[16]}$ $-3.4(0.6)^{[16]}$ $-3.70(0.08)^{[16]}$	
Q_{mat} (fm^2)	-3.99	$-4.1(0.6)^{[16]}$ $-4.00(0.06)^{[16]}$	$-3.82^{[10]}$ $-3.83^{[10]}$ $-4.41^{[10]}$
$B(E2, \frac{3}{2}^- \to \frac{1}{2}^-)$ (e^{2}fm^4)	7.55	$8.3(0.6)^{[16]}$ $8.3(0.5)^{[16]}$ $7.59(0.12)^{[19]}$ $7.27(0.12)^{[19]}$	$7.74^{[10]}$ $7.75^{[10]}$ $10.57^{[21]}$
$B(M1, \frac{3}{2}^- \to \frac{1}{2}^-)$ (μ^2)	2.45	$2.50(0.12)^{[16]}$	
$\Gamma(\frac{7}{2}^-)$ (keV)	~ 110	$93(8)^{[20]}$	
$\Gamma(\frac{5}{2}^-)$ (keV)	~ 930	875^{+200}_{-100}	

contains, besides the Coulomb repulsion (corrected at small distances for the sphericity of charge distributions), the nuclear attractive potential (assumed of simple Woods-Saxon form) and the spin-orbit term [17]. The depth of the Woods-Saxon well ($V_{WS} = -74.923$ MeV) and the magnitude of the spin-orbit correction ($V_{ls} = 1.934$ MeV) have been adjusted to reproduce the energy eigenvalues for the two bound states. The α cluster has spin 0 while the t cluster has spin $\frac{1}{2}$. The angular momentum coupling between the $\ell = 1$ relative motion and the spin of the triton provides the total angular momenta $(\frac{3}{2})^-$ for the ground states with energy -2.467 MeV and $(\frac{1}{2})^-$ for the first excited state at -1.989 MeV [18]. (Energies are measured with respect to the α-t breakup threshold.) The resulting wave functions for the ground state and for the first excited state are in a qualitative agreement with the ones obtained in the paper of Wallisser and Fliessbach (for example, the radial node occurs at the same point).

In spite of its simplicity, this model for ^{7}Li is nevertheless capable of a good agreement with experimental observations, as witnessed by the list of observables in table 1 [16,19–22]. Evaluation of charge radius, electric and matter quadrupole moments, $B(E2)$ and $B(M1)$ values for transitions between the ground state and the first-excited state are reported. These quantities, except the two width, are calculated according to the prescriptions given in ref. [16]. These observables are very sensitive to the particular shape of the wave functions and therefore

provide a reliability test for our approach as far as boun states are concerned. In the same table we also compar our findings with previous calculations. The last two row in the table refer to the widths of the two $f_{7/2}$ and $f_{5/}$ resonances which are given with the purpose to show tha this model gives also sensible predictions for the contir uum states.

3 Electromagnetic response

We now apply the dicluster picture to the calculation c electromagnetic response for the transitions to continuu states. In this scheme all the features of the transition ar ascribed to the modification of the wave functions describ ing the relative motion. The clusters are in fact assume to be frozen in this picture, and their intrinsic wave func tions are not modified by the electromagnetic operator: The multipole operator may be written as a sum of oper ators that act on different degrees of freedom. Since ther is no rearrangement of the intrinsic structure of the tw clusters, the corresponding parts will not contribute to the $B(E\lambda)$. The strength distribution for the transition from an initial state of the intrinsic motion with wave function $\psi_{n_i l_i}(r)$ and quantum numbers n_i, l_i, j_i to a different final state (either bound or unbound) with wave function $\psi_{n_f l_f}(r)$ and quantum numbers n_f, l_f, j_f may be written as

$$B(E\lambda) = \frac{\hat{j_f}^2 \hat{l_f}^2 \hat{l_i}^2 \hat{\lambda}^2}{4\pi} e_\lambda^2 \begin{pmatrix} l_f & \lambda & l_i \\ 0 & 0 & 0 \end{pmatrix}^2 \begin{Bmatrix} l_f & j_f & j_{cl} \\ j_i & l_i & \lambda \end{Bmatrix}^2 \cdot \left(\int_0^\infty \psi_{n_f l_f}(r) r^{\lambda+2} \psi_{n_i l_i}(r) \mathrm{d}r \right)^2 , \quad (3.1)$$

where $\hat{j} = (2j+1)^{1/2}$ and the effective charge is defined as $e_\lambda = Z_{cl}(A_{co}/A)^\lambda + Z_{co}(-A_{cl}/A)^\lambda$ and the subscripts cl and co refer to the cluster (the one with a nonzero intrinsic angular momentum) and the core (the one with a null intrinsic angular momentum). When the final state is in the continuum, its wave function also depends on E_C.

Starting from the ground state (with p character) we have investigated electric dipole transitions to s and d states as well as quadrupole transitions to p and f states. The corresponding differential transition probabilities are shown in figs. 1. In the former case, the scattering states for even multipolarities have been calculated with the same potential that has been used to generate the bound states. In the latter case, the same parameters have been used for the p-wave continuum, while for the f-wave modified Woods-Saxon ($V_{WS} = -68.255$) and spin-orbit ($V_{ls} = 3.115$) potentials have been used to yield the $7/2^-$ and $5/2^-$ resonant states in the excitation spectrum at the correct energy. With this choice the widths of these two states have been found in reasonable agreement with experimental observations as shown in the last part of table 1, without the need for further adjustments. Besides this resonant strength we observed a concentration of strength of non-resonant character at the separation

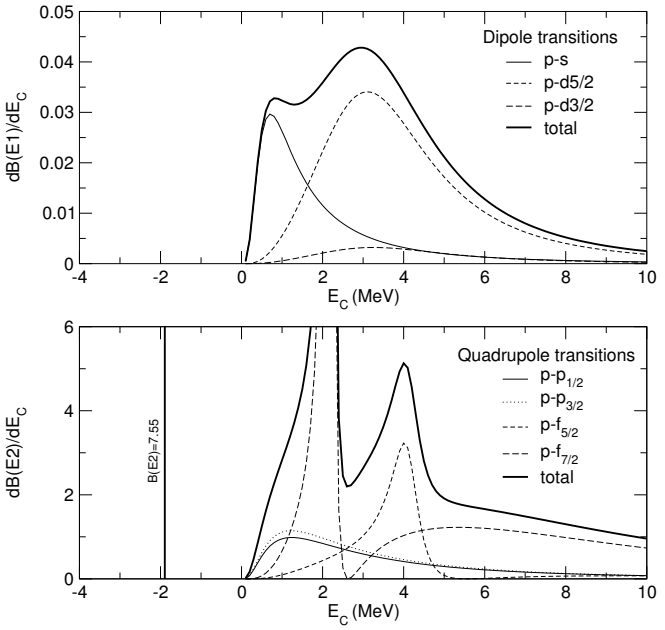

Fig. 1. Upper panel: differential $B(E1)$ values (in $\mathrm{e}^2\,\mathrm{fm}^2/\mathrm{MeV}$) for transitions from the ground state to the continuum. Energies are in MeV, the different contributions are indicated in the legend. Lower panel: differential $B(E2)$ values (in $\mathrm{e}^2\,\mathrm{fm}^4/\mathrm{MeV}$) for transitions from the ground state to the continuum and to the first-excited bound state, displayed in the figure as a discrete bar (the transition strength is indicated). Energies are in MeV, referred to the threshold for breakup into the α-t channel.

threshold, solely due to the weakly bound nature of the ^{7}Li nucleus. This strength is small for multipolarities that have a resonance in the low-lying continuum, but it is sizable when there are no resonances (as in the p cases).

We have compared our calculated values with the predictions of the energy-weighted sum rules as well as of the energy-weighted molecular sum rules (EWMSR) [23, 24], also called AGB sum rule, that are particularly useful for molecular-like structures. In light nuclei enhanced $E1$ transitions have been observed for which $B(E1)$ values may still be very small in comparison with single-particle estimates. EWMSR have been introduced as a measure for these transitions and in the cases of dipole and quadrupole they read

$$S_I(E1, A_1 + A_2) = \left(\frac{9}{4\pi}\right) \frac{(Z_1 A_2 - Z_2 A_1)^2}{A A_1 A_2} \left(\frac{\hbar^2 e^2}{2m}\right) \quad (3.2)$$

and

$$S_I(E2, A_1 + A_2) = \left(\frac{25}{2\pi}\right) \frac{1}{Z} \left(Z_1 Z_2 + \left(Z_1 \frac{A_2}{A} - Z_2 \frac{A_1}{A} \right)^2 \right) S_0^2 \left(\frac{\hbar^2 e^2}{2m}\right) , \quad (3.3)$$

under the assumption that the nucleus with mass A and charge Z is split into two clusters with masses A_1 and A_2, charges Z_1 and Z_2 and neutron numbers N_1 and N_2.

The distance S_0 is the equilibrium separation that may be simply calculated as the sum of the radii of the two clusters (we have taken $S_0 = 3.63$ fm). We find that the low-lying dipole strength exhausts approximatively the 2.6% of the Thomas-Reiche-Kuhn sum rule, but it amounts to about 94% of the energy-weighted molecular dipole sum rule. Similarly, the quadrupole strength is the 9.2% of the energy-weighted quadrupole sum rule and about 42% of the EWMSR. For a proper comparison with the sum rule, we have included in the calculation of the exhausted fraction of sum rules, besides the transition to the continuum and the quadrupole transition to the first-excited state, all the possible transitions to lower unphysical bound states ($1s_{1/2}, 2s_{1/2}, 1d_{5/2}, 1d_{3/2}$ for dipole and $1p_{3/2}, 1p_{1/2}$ for quadrupole). Note that the dipole transitions to unphysical states give a negative contribution of about 50% to the total energy-weighted strength.

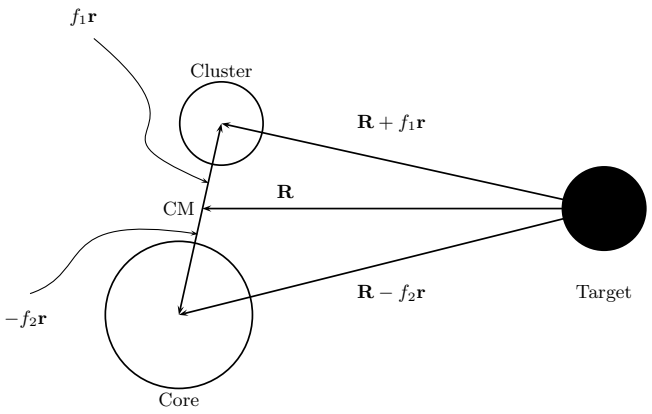

Fig. 2. Coordinate system for the interaction between a dicluster nucleus (white) and an external target (black).

4 Formalism and form factors

We move now from the pure electromagnetic response to the study of the breakup reaction in which the dicluster ^{7}Li nucleus is used as a projectile on a heavy target.

The coordinate system for the interaction between a dicluster nucleus and a target is depicted in fig. 2. The factors f_1 and f_2 are the ratios of the distances of the center of mass of each cluster from the common center of mass divided by the inter-cluster distance r. We have named the two clusters as "core" and "cluster" to avoid confusions even if the alpha particle has not a mass large enough to justify the choice with respect to the triton.

Within the cluster model, the wave function for ^{7}Li is the product of the wave functions of the two alpha and triton clusters (assumed to be frozen during the transition) and of the wave function describing the relative cluster-cluster motion. Assuming a value L for the relative angular momentum, and taking into account the intrinsic $j = 0$ and $j = 1/2$ spins for the alpha and the triton, the generic state with total spin J can be expressed as $\mid L, J, M\rangle$. For states in the continuum, states are also characterized by the value E_C of the energy in the continuum, namely $\mid L, J, M; E_C\rangle$. The form factor associated with a process in which the relative cluster-cluster motion undergoes a transition to the continuum is given by

$$F(\mathbf{R}, E_C)_{LJM\to L'J'M';E_C} = \langle L'J'M'; E_C \,|\, V(\mathbf{R}, \mathbf{r}) \,|\, LJM\rangle \tag{4.1}$$

in terms of the relative projectile-target coordinate $\mathbf{R}$. The relevant interaction is assumed as the sum of the interactions of the target, labeled with T, with each cluster,

$$V(\mathbf{R}, \mathbf{r}) = V_{\alpha-T}(\mid \mathbf{R} - f_2\mathbf{r} \mid) + V_{t-T}(\mid \mathbf{R} + f_1\mathbf{r} \mid), \tag{4.2}$$

where each interaction consists in a nuclear and a Coulomb part, the former being assumed to be of a Woods-Saxon form. Since the clusters are frozen during the transition the integration over the internal degrees of freedom is straightforward and one is left with an integration over the cluster-cluster coordinate $\mathbf{r}$ in the form

$$\begin{aligned} F(\mathbf{R}, E_C)_{LJM\to L'J'M';E_C} &= \sqrt{\pi}\hat{J}\hat{J}'\hat{L}\hat{L}' \\ &\times \sum_{\lambda,\mu}(-1)^{3j_{cl}-M'} \begin{pmatrix} J & J' & \lambda \\ -M & M' & \mu \end{pmatrix} \begin{pmatrix} L' & L & \lambda \\ 0 & 0 & 0 \end{pmatrix} \begin{Bmatrix} J' & J & \lambda \\ L & L' & j_{cl} \end{Bmatrix} \\ &\times \left[\int_0^\infty r^2 \mathrm{d}r \int_{-1}^{1} \mathrm{d}u \psi_L(r) \psi_{L',E_C}(r) \Big(V_{\alpha-T}(\mid \mathbf{R} - f_2\mathbf{r} \mid) \right. \\ &\left. + V_{t-T}(\mid \mathbf{R} + f_1\mathbf{r} \mid) \Big) P_\lambda(u) \right] Y_{\lambda,\mu}(\hat{R}), \end{aligned} \tag{4.3}$$

where λ, μ are the change in orbital angular momentum and its third component due to the transition and u is the cosine of the angle between the two vectors $\mathbf{R}$ and $\mathbf{r}$. As in the previous section, $\hat{j} = (2j+1)^{1/2}$.

The resulting Coulomb and nuclear form factors for the ^{7}Li + ^{165}Ho reaction are plotted in fig. 3 for a dipole transition between the $p_{3/2}$ ground state and the $s_{1/2}$ state at $E_C = 1$ MeV in the continuum. It is evident that the nuclear field dominates at smaller distances, while the Coulomb one dominates at larger distances. This is once again displayed in the next three figures where three different distances have been kept constant and the Q-value dependence upon E_C is illustrated. The nuclear contribution is still very important at a distance of 12–14 fm that is far beyond the geometrical sum of the radii of the two systems. This effect may even be magnified in halo systems closer to the drip lines, where the weakly bound wave functions are even more extended. Figures of qualitatively similar behaviour are obtained for all the other possible transitions.

To better understand the relative role of dipole and quadrupole interactions, we show separately in fig. 4 the form factors for selected dipole and quadrupole transitions. Together with the total form factor, we report the contribution arising from the interaction between each of the two clusters and the target separately. In the case of a dipole transition a cancellation occurs between the two contributions, while for the quadrupole case the two

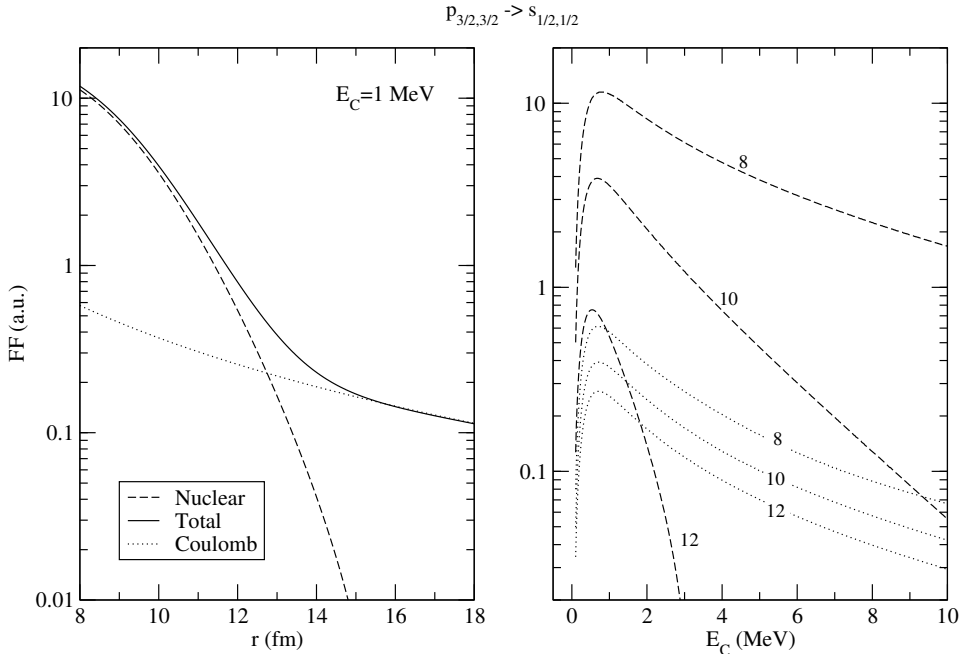

Fig. 3. Form factors (in arbitrary units) for a particular transition plotted against the distance, for a fixed energy in the continuum of $E_C = 1\,\mathrm{MeV}$ (left panel, logarithmic vertical scale) and against the energy in the continuum for three fixed distances (right panel). Coulomb (dotted) and nuclear (dashed) form factors are shown. See text for details.

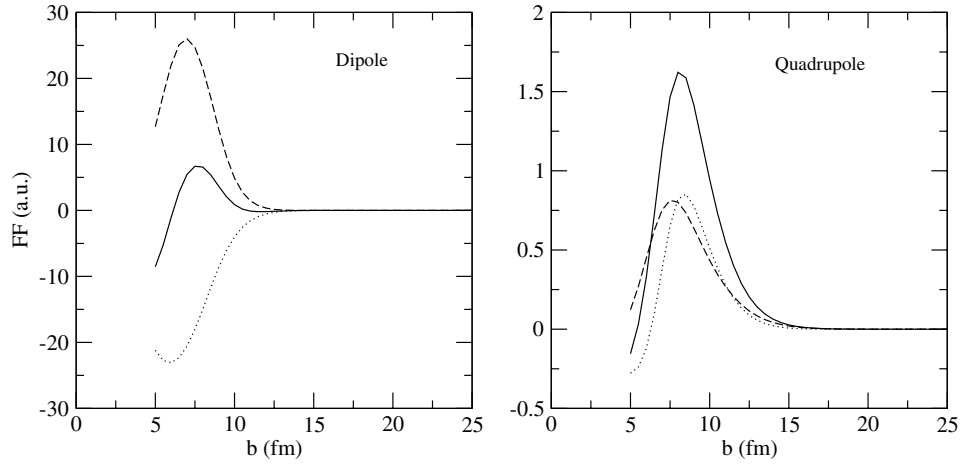

Fig. 4. Form factors for dipole and quadrupole cases as a function of the distance r for the transition $p_{3/2,3/2} \rightarrow s_{1/2,1/2}$ for an excitation energy in the continuum $E_C = 1\,\mathrm{MeV}$. The three different curves correspond to ^{7}Li-target (solid line), α-target (dotted) and t-target interactions.

clusters contribute constructively to the excitation. The effect is here amplified by the fact that the two clusters have similar sizes. In the limit of two equal clusters, the nuclear contribution to dipole transitions would exactly vanish. Similarly, no Coulomb dipole transitions are allowed if the two clusters have equal mass-to-charge ratios.

5 Cross-section

The form factors obtained in the last section contain all the relevant elements to build up breakup cross-sections and Q-value distributions in a simple, although accurate procedure. The reaction amplitudes can be calculated in a semiclassical coupled-channel approach. The energy in the continuum is divided in a suitable number of intervals, treated as different channels. For each energy interval (and each spin), the form factor connecting with the ground state is obtained (assuming the central value of the energy interval) as described in the previous section. To keep simple the calculations continuum-continuum couplings have not been included, although in some cases they were found to play a relevant role (see, for example, ref. [25]). We follow in time the solutions of the system of coupled equations for the amplitudes in the different channels, along a trajectory that is calculated semiclassically

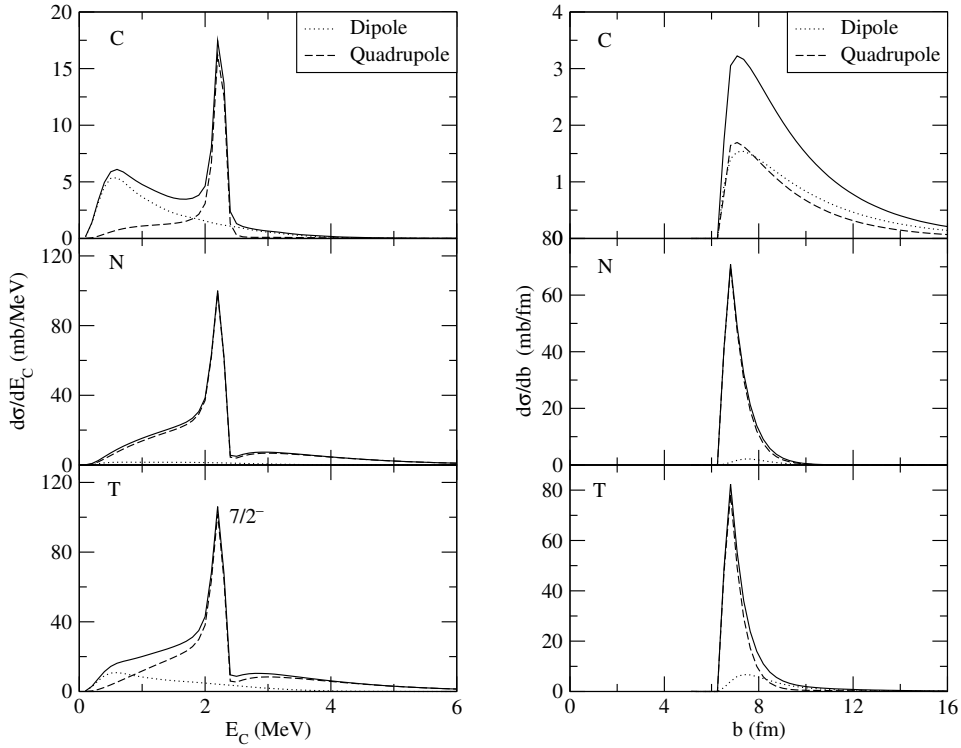

Fig. 5. Left panels: Q-value distribution for (Coulomb, nuclear and total or interference) breakup of ^{7}Li on ^{165}Ho at $E_{cm} =$ 40 MeV. Dipole (dotted) and quadrupole (dashed) contributions are shown together with their sum (full line). The $7/2^-$ resonance is marked, while the $5/2^-$ around 4 MeV is very small. Right panels: differential (Coulomb, nuclear and total) breakup cross-sections as a function of the impact parameter with the same data of the left figures. Again different multipolarities are shown separately and one may notice the different behaviour at large impact parameter, that is dominated by the dipole contribution.

using a standard Akyuz-Winther parameterization [26] for the target-projectile potential. The values of the amplitudes at the end of the scattering process are then used to calculate cross-sections for the excitation of a given channel and differential cross-sections as a function of the energy in the continuum. The simplicity of the scheme allows us to use a rather small energy mesh, without any convergence problem as the mesh is reduced. This is particularly important when one has to deal with a continuum that includes, as in our case, narrow resonances. Details on the formalism may be found in ref. [2]. The resulting cross-sections are collected in fig. 5. The Q-value distribution obtained for Coulomb breakup is displayed in left-upper panel (the contributions of the dipole and quadrupole transitions are separately shown, together with their sum). It is worthwhile noticing that the two low-lying peaks arise from different mechanisms: the peak at around 0.5 MeV is mostly built up with transitions to the continuum which are enhanced due to the weak-binding nature of the projectile, while the peak at 2.186 MeV has a true resonant nature ($7/2^-$). In the case of quadrupole transition the non-resonant strength can be less easily seen just above the threshold, since the different radial dependence of the form factor makes its relative magnitude small compared to the dipole one, in spite of a larger value of the $B(E\lambda)$'s distribution. Differential cross-sections with respect to impact parameter are also shown in the right column of fig. 5. At low impact parameters the excitation process is strongly quenched by the transmission factor. For large values one can see the different behaviour of the two tails: the quadrupole contribution decays faster than the dipole. Consequently, at large impact parameters, that, in a classical picture, correspond to forward angles, the Coulomb breakup cross-sections are mostly due to dipole transitions to the continuum. The total Coulomb cross-section (resonant and non-resonant) at $E_{cm} = 40$ MeV amounts to ~ 4.85 mb, with comparable dipole and quadrupole contributions (~ 3.0 mb for the dipole and ~ 1.85 mb for the quadrupole).

To evaluate the effect of the nuclear interaction we need to specify the precise set of optical parameters between each of the two clusters and the target nucleus. We have looked up for optical parameters in the standard tables [27,28], where data sets for elastic scattering on holmium are missing, and, in absence of any alternative, we have used parameters extracted for cerium, which is the closest isotope. We used only the real part of the potentials in the construction of the form factors. Of course we do not expect these parameters to represent a strictly valid quantitative choice, but we have used them in order to give estimates of the nuclear and total breakup cross-sections that are reported in the following. The nuclear breakup has a Q-value distribution (depicted in fig. 5, second row of the left column) with an overall profile that resembles

Table 2. Cross-sections for the breakup of ^{7}Li into $\alpha + t$ cluster states in the ^{7}Li + ^{208}Pb reaction at $E = 48$ MeV. The contributions arising from final states with given angular momentum (L') are separately listed.

	$\sigma(^7\mathrm{Li} \to \alpha + t)$ (mb)	
$L'(\hbar)$	Ref. [8]	This work
0	26.3	22.9
1	6.0	4.4
2	–	25.3
3	15.9	6.7
Total	48.2	59.3

the Coulomb one, being the total integrated cross-section about ~ 24.1 mb. At variance with previous findings the dipole contribution to this cross-section (~ 1.3 mb) is now much smaller that the quadrupole one (~ 22.8 mb). This is again originated by the comparable size of the clusters, that hinders dipole components, while the predominant nuclear quadrupole term is not quenched by the faster radial dependence of the form factor as in the case of the Coulomb term. In this case, therefore, both resonant and non-resonant peaks are of predominant quadrupole nature.

The final Q-value distribution and the corresponding curve as a function of the impact parameter, both taking into account the interference between the two fields, are depicted in the last row of fig. 5. The total cross-section amounts to about ~ 29.0 mb. The dipole transition contributes for ~ 6.9 mb, while the quadrupole is about ~ 22.1 mb. It should be noticed that, while the Coulomb contribution is rather insensitive to the absorption radius, a significant change in the nuclear cross-section (and therefore in the total one) may occur as long as the radius of the nuclear interaction is varied, as as one can easily infer, for example, from the last panel. For a discussion on the subject, see for example ref. [2].

In order to test our model and to compare with other available models we have performed calculations of breakup cross-sections for ^{7}Li on ^{208}Pb at 48 MeV bombarding energy. Our calculations may be directly confronted with the work of Kelly and collaborators [8], that are essentially based on the same physical ingredients. We report both theirs and our results in table 2. Standing the differences in the values of the couplings (we extracted ^{208}Pb-α and ^{208}Pb-t optical parameters from the work of Gupta *et al.* [29]) and in the treatment of the continuum (we take into account continuum energy up to 10 MeV), the agreement among the various contributions to the cross-sections from $\lambda = 0, 1$ and 3 states is satisfactory, although some discrepancy is seen in the $\lambda = 3$ continuum. In addition, we provide calculations for the contribution arising from d states, that is found to be a very important component of the total cross-section. This is at variance with respect to the cited analysis by Kelly *et al.*, where the quadrupole component is considered to be negligible. The numerical results in table 2 have been obtained considering dipole and quadrupole transitions only, but we have checked that octupole transitions to d states and hexadecupole transitions to f states may be neglected (being around 10^{-3}mb and 0.9 mb, respectively).

6 Conclusions

We have illustrated a general model to describe excitations to continuum states in weakly bound dicluster nuclei, leading to cluster dissociation. In the model the internal degrees of freedom of the clusters are kept frozen in the excitations, which are therefore entirely ascribed to the relative cluster-cluster motion. Both resonant and non-resonant continuum states are simultaneously properly included. In the case of weakly bound nuclei the non-resonant part shows the presence of multipole strength at the threshold that is a typical feature for single-particle excitations in one-particle halo nuclei.

Paralleling the formalism previously developed for the breakup of one-particle halo nuclei, form factors for transitions to cluster continuum states are constructed and cross-sections for cluster breakup reactions are calculated in a semiclassical coupled-channel description. The interplay of dissociation via resonant states or via non-resonant continuum is discussed. The form factors are studied in detail: we illustrate their behaviour as a function of the relative distance of the two colliding nuclei, as a function of the energy of the continuum states and we discuss the effects of cancellation and reinforcement, for dipole and quadrupole transitions, respectively, that is a consequence of the relative masses and charges of the two clusters.

Q-value distributions and differential breakup cross-sections with respect to impact parameters, as well as the total breakup cross-sections, are evaluated for the reaction ^{7}Li + ^{165}Ho, taking into account both nuclear and Coulomb contributions, although restricted to dicluster nuclei. This simple approach to the breakup problem avoids possible problems arising from a crude energy binning of the continuum. Our results show that, in the case of a system described in terms of two clusters of similar size and charge (as is the case of ^{7}Li), the main contribution to breakup processes come from the nuclear quadrupole mechanism.

The authors acknowledge fruitful discussions with K. Hagino and C.H. Dasso.

References

1. F. Catara, C.H. Dasso, A. Vitturi, Nucl. Phys. A **602**, 181 (1996).
2. C.H. Dasso, S.M. Lenzi, A. Vitturi, Nucl. Phys. A **639**, 635 (1998).
3. I. Hamamoto, H. Sagawa, X.Z. Zhang, Phys. Rev. C **53**, 765 (1996); I. Hamamoto, H. Sagawa, Phys. Rev. C **53**, R1492 (1996); I. Hamamoto, H. Sagawa, X.Z. Zhang, Phys. Rev. C **57**, R1064 (1998).

4. J. Al-Khalili, F. Nunes, J. Phys. G **29**, (2003), R89.
5. S. Typel, G. Baur, nucl-th/0411069.
6. M.A. Nagarajan, S.M. Lenzi, A. Vitturi, Eur. J. Phys. A **24**, 63 (2005).
7. C.H. Dasso, S.M. Lenzi, A. Vitturi, Nucl. Phys. A **611**, 124 (1996).
8. G.R. Kelly *et al.*, Phys. Rev. C **63**, 024601 (2000).
9. C. Signorini *et al.*, Eur. J. Phys. A **10**, 249 (2001).
10. M. Dasgupta *et al.*, Phys. Rev. C **66**, 041602(R) (2002).
11. M. Mazzocco *et al.*, Eur. J. Phys. A **18**, 583 (2003).
12. M. Yahiro *et al.*, Prog. Theor. Phys. **67**, 1464 (1982); F.M. Nunes, I.J. Thompson, Phys. Rev. C **59**, 2652 (2000).
13. N. Keeley, K.W. Kemper, K. Rusek, Phys. Rev. C **66**, 044605 (2002); N.J. Davis *et al.*, Phys. Rev. C **52**, 3201 (1995).
14. V. Tripathi *et al.*, Phys. Rev. Lett. **88**, 172701 (2002).
15. J.E. Mason *et al.*, Phys. Rev. C **45**, 2870 (1992).
16. H. Walliser, T. Fliessbach, Phys. Rev. C **31**, 2242 (1985).
17. A. Bohr, B.R. Mottelson, *Nuclear Structure* (W.A. Benjamin, Inc., New York, Amsterdam, 1969).
18. D.R. Tilley *et al.*, Nucl. Phys. A **708**, 3 (2002).
19. H.G. Voelk, D. Fick, Nucl. Phys. A **530**, 475 (1991).
20. Y. Tokimoto *et al.*, Phys. Rev. C **63**, 035801 (2001).
21. B. Buck, A.C. Merchant, J. Phys. G **14**, L211 (1988).
22. T. Kajino, Nucl. Phys. **460**, 559 (1986).
23. Y. Alhassid, M. Gai, G.F. Bertsch, Phys. Rev. Lett. **49**, 1482 (1982).
24. H.J. Assenbaum, K. Langanke, A. Weiguny, Phys. Rev. C **35**, 755 (1987).
25. F.M. Nunes *et al.*, Nucl. Phys. A **736**, 255 (2004).
26. R.A. Broglia, A. Winther, *Heavy Ion Reactions* (Addison-Wesley, Redwood City, 1991).
27. C.M. Perey, F.G. Perey, At. Data Nucl. Data Tables **17**, 1 (1976).
28. R.P. Ward, P.R. Hayes, At. Data Nucl. Data Tables **49**, 316 (1991).
29. D. Gupta *et al.*, Nucl. Phys. **646**, 161 (1999); **683**, 3 (2001).